



Atomistic to continuum mechanics description of crystal defects with dislocation density fields: Application to dislocations and grain boundaries

Houssam Kharouji^a, Lucile Dezerd^b, Pierre Hirel^c, Philippe Carrez^c, Patrick Cordier^{c,d}, Vincent Taupin^a, Julien Guénolé^{a,*}

^a Université de Lorraine, CNRS, Arts et Métiers, LEM3, F-57070 Metz, France

^b Institut Jean Lamour, CNRS UMR 7189, Université de Lorraine, F-54000 Nancy, France

^c Université de Lille, CNRS, INRAE, Centrale Lille, UMET, F-59000 Lille, France

^d Institut Universitaire de France, F-75005 Paris, France

ARTICLE INFO

Keywords:

Dislocations
Grain boundaries
Nye tensor
Ab-Initio
Molecular Statics
Field Dislocation Mechanics

ABSTRACT

The atomic structure of crystal defects such as dislocations, grain or phase boundaries, control these defects' properties: their mobility, ability to cross-slip, or solute segregation. These crystal defects can be conveniently studied by atomistic simulations and one then needs to transfer relevant information at the upper scale to model microstructures containing a large number of defects, e.g., a polycrystal. Here, we propose an atomistic to continuum mechanics crossover method that (i) represents the atomic structure of dislocations cores by an appropriate Nye dislocation density tensor field and (ii), captures quantitatively the short and long range mechanical fields of defects. For (i), we propose a modified and improved interpolation method based on the original work by Hartley and Mishin. For (ii), we use a field dislocation mechanics framework that rigorously calculates/evaluates the mechanical fields associated with any Nye dislocation density distribution. The transfer method relies on molecular static calculations using two energetic models — ab-initio for screw dislocation core simulations in tungsten, and EAM potential for low and large angle grain boundaries in copper. Our findings demonstrate the effectiveness of the proposed approach in reconstructing the Burgers vector, and continuous strain and rotation fields. The framework is further applied to analyze the elastic interactions between extrinsic edge dislocations and a low angle grain boundary in copper.

1. Introduction

Crystal defects, in particular dislocations and grain boundaries (GBs), are well known to control the mechanical properties of crystalline materials. A thorough understanding of these defects is essential for designing materials with mechanical properties tailored for a wide range of applications (Bertin et al., 2020). Dislocation and GB physics is a multidisciplinary field that investigates the behavior and properties of defects across a broad spectrum of scales, from the atomic-level where, for instance, the dislocation core involves a few atoms only, up to the scale of polycrystals where billions of dislocation lines interact with each others and with GBs. At the atomic scale, Molecular Dynamics/Statics (MD/MS) simulations are widely used to model the fundamental structures and properties of dislocations or GBs. These simulations provide detailed and quantitative insights on defected atomic configurations,

* Corresponding author.

E-mail address: julien.guenole@univ-lorraine.fr (J. Guénolé).

<https://doi.org/10.1016/j.ijplas.2024.103990>

Received 23 February 2024; Received in revised form 30 April 2024

Available online 3 May 2024

0749-6419/© 2024 The Author(s). Published by Elsevier Ltd. This is an open access article under the CC BY license (<http://creativecommons.org/licenses/by/4.0/>).

energies, mobilities, etc. Xu et al. (2022), Weinberger and Tucker (2016). They are also widely used to predict the interactions between dislocations and grain boundaries, and discern configurations that facilitate dislocation absorption or transmission through grain boundaries in metallic materials (Borodin et al., 2020). Nonetheless, atomistic simulations are usually limited to small time and size scales, typically of the order of few nanoseconds and tens of nanometers. As such, multiscale efforts are needed to extract relevant physical and mechanical information from atomistic simulations, and incorporate it in larger scale models, in order to simulate realistic and statistically meaningful microstructures. Such larger scale modeling approaches are discrete dislocation dynamics (Espinosa et al., 2006; Lu et al., 2022), phase field models (Miehe et al., 2016; Jafari et al., 2017), or continuum mechanics based crystal defect models (Jebahi et al., 2020).

Continuum mechanics approaches are well suited for tracking the evolution of mechanical fields and defected microstructures (elastic/plastic deformation, internal stresses, dislocation densities etc.) at the mesoscale, i.e., at the scale of grains. Frank and Bilby were pioneers in the development of such fundamental theories for mechanically representing the structure of grain and phase boundaries (Frank, 1950; Priestler, 2012). The continuous approach they proposed describes the interface as a dislocation surface density, more precisely by a Burgers vector density, that accommodates the incompatibility of elastic transformation at the interface (Priester, 2012). This model was later adopted by Read and Shockley to establish a correlation between the excess energy of GBs and their misorientation angle (Read and Shockley, 1950). Recently, this model has seen extensions to more general grain boundaries. It was shown that a link between misorientation, Burgers vector content of grain boundaries, and GB excess energy, can be established for a broad spectrum of misorientations and GB types using a generalized Read and Shockley model (Van Beers et al., 2015). The Frank and Bilby model has also been successfully applied to investigate the migration of tilt GBs in a mean-field micromechanical framework (Berbenni et al., 2013). In a similar context, phase field approaches have demonstrated their ability to study various aspects of crystal elasticity (Heinonen et al., 2014), dislocation mobility (Berry et al., 2014), and deformation twinning in crystalline materials (Trautt et al., 2012). Phase field models can be enriched by incorporating information from atomistic simulations. For instance, stacking fault energies as obtained from density functional theory (DFT) calculations can be introduced, which allows to model the dissociated structures and mobility of dislocation cores (Beyerlein and Hunter, 2016).

The field dislocation mechanics (FDM) model considered in the present work is a somewhat alternative to dislocation phase field models at small scales (Acharya, 2001). This approach provides a continuous representation of dislocation cores using an appropriate distribution of dislocation density. It relies on the Nye dislocation density tensor (Nye, 1953), the Kröner incompatibility equation (Kröner, 1980), and the dislocation density transport equation (Mura, 1963). One of the primary advantages of this model is its ability to provide a fully continuous description of crystalline defects using Nye dislocation densities, which enables to model dislocation core structures (Zhang et al., 2015). The presence of a Nye dislocation density is linked to an incompatible elastic distortion and generates internal stresses. Although the FDM approach can be applied to dislocations and grain boundaries, the introduction of disclination fields (Fressengeas et al., 2011) was proposed to offer an alternative description of such grain boundaries. This model has been successfully applied to tilt GBs (Taupin et al., 2013) and twist interfaces (Guénolé et al., 2022). It notably enables the reproduction of structural units that compose grain boundaries, their excess energy (Fressengeas et al., 2014) and their migration kinematics (Taupin et al., 2014). Disclination and/or dislocation density approaches thus allow for the substitution of the atomic structure of defects (such as dislocations and interfaces) for an equivalent representation using defect densities, thereby enabling their incorporation into a continuum mechanics framework for upscaling. In addition to being predictive, FDM has previously been compared to analytical solutions, in the case of single dislocations, dislocations near pores and inclusions (Berbenni et al., 2014; Djaka et al., 2017). Additionally, other dislocation models using gradient elasticity to regularize singularities at the dislocation cores were validated by comparison with molecular statics (Seif et al., 2015).

Based on the framework presented above, we have developed a novel method for an atomistic to continuum mechanics crossover with the objective of capturing the core structure and the continuous mechanical fields of various crystal defects, including dislocations and grain boundaries. We restrict ourselves to field dislocation mechanics here, but the approach can be extended to incorporate disclination fields. Our approach thus involves the description of the atomic structure of crystal defect cores in terms of an equivalent Nye dislocation density. The first stage entails computing the per-atom elastic distortion field from atomistic simulations, the incompatible part of which yields the associated Nye dislocation density. For this task, we are using the Hartley Mishin algorithm (Hartley and Mishin, 2005) that provides the inverse elastic transformation (also called correspondence tensor) as well as the Nye density on each atom in an atomistic configuration. For the second stage, we explore the appropriate metrics, whether it be the per-atom inverse elastic transformation or directly the per-atom Nye tensor, to perform our transition from atomistic data to our continuum mechanics FDM model. More precisely, as our FDM model field equations are numerically approximated on a regular fast Fourier transform (FFT) grid, we try different interpolations of atomistic data (transformation or Nye tensors) onto the FFT grid and compare with atomistic data in terms of Burgers vector and short/long range mechanical fields (elastic strains and rotations). We assess our atomistic to continuum mechanics crossover by the ability of the atomistic-aided FDM to predict the elastic fields of different defects. Defects include screw dislocations dipoles, edge dislocations array and structural units in high angle tilt grain boundaries.

The structure of this paper can be summarized as follows. First, we provide an initial overview of the atomistic methods employed for simulating crystal defects (Section 2). This includes Density Functional Theory (DFT) methods to model $1/2[1\ 1\ 1]$ screw dislocation dipoles in tungsten and Molecular Statics (MS) for producing high and low-angle tilt grain boundaries in copper. In our study, the choice to employ distinct atomistic scale simulation methods for tungsten and copper stems from their difference in terms of crystal structures and mechanical properties and response. Ab-initio simulations accurately capture screw dislocation with cores in BCC Fe by considering the electronic effects, but are computationally intensive. For larger scale simulations, molecular statics using semi-empirical potentials offers a computationally efficient alternative, yet sufficiently accurate. Following this, a brief

overview of dislocation mechanics allows us to introduce the Hartley and Mishin algorithm used to compute the per-atom lattice correspondence and Nye tensors. The latter part of Section 2 is devoted to elucidating the method employed for transitioning from atomistic data to our continuous mechanical model. Section 3 is dedicated to applications of the crossover method, where we systematically assess the ability of FDM to reproduce the Burgers vector of defects and their mechanical fields. The final part of Section 3 is focused on applying the transfer method to investigate the interactions between extrinsic edge dislocations and a low angle tilt grain boundary. Section 4 concludes our study and presents further directions.

2. Methods

2.1. Numerical simulation methods

2.1.1. Atomistic approaches

Ab-initio calculations based on the density functional theory (DFT) were performed to simulate the core structure of $1/2[111]$ screw dislocations in body-centered cubic (BCC) tungsten. All computations were carried out using the Vienna ab-initio simulation package (VASP) (Kresse and Hafner, 1993). The exchange–correlation interactions were described using the Generalized Gradient Approximation (GGA) with the Perdew–Burke–Ernzerhof (PBE) parametrization. A screw dislocation dipole is inserted within a supercell containing 135 atoms with three-dimensional (3D) periodic boundary conditions using periodicity vectors $\vec{C}_1 = 5/2[1\bar{2}1] + 9/2[\bar{1}01]$, $\vec{C}_2 = 5/2[1\bar{2}1] - 9/2[\bar{1}01]$, and $\vec{C}_3 = 1/2[111] = \vec{b}$ as presented in the recent work of Bienvenu et al. (2022), Clouet et al. (2021), Bienvenu et al. (2020) (See Figure S1 in Supplementary Material). We set a kinetic energy cutoff of 400 eV for the plane-wave basis and convergence criterion of 0.05 eV/Å on the forces for ionic relaxations.

To simulate symmetric tilt GBs in face-centered cubic (FCC) copper, we employed the Molecular Dynamics LAMMPS code (Thompson et al., 2022). The atomic interactions were modeled using the embedded atom method (EAM) potential of Mishin et al. (2001) for Cu. This potential accurately predicts key physical properties of Cu, including the lattice parameter, cohesive energy, vacancy formation energy, GB excess energies and elastic stiffness moduli. In this study, we consider the low-angle grain boundary (LAGB) $\Sigma 365(27\ -1\ 0)[001]4.24^\circ$ and the high-angle grain boundary (HAGB) $\Sigma 5(310)[100]36.8^\circ$. Figure S2 (supplementary material) illustrates the simulation boxes for each of these GBs. Note that each computational cell contains two opposite grain boundaries because of periodic boundary conditions. The simulation cell dimensions for LAGB and HAGB are $(137 \times 252 \times 3.615 \text{ Å}^3)$ and $(293 \times 391 \times 3.615 \text{ Å}^3)$, respectively. These dimensions are sufficiently large to prevent any significant interaction between the two opposite grain boundaries. Molecular Statics (MS) calculations were performed to determine the minimum energy configuration of each grain boundary. The standard simulation methodology includes rigid body translation of rotated grains, application of atom deletion criteria and the use of the conjugate gradient method for relaxing the initial atomic structures. The details of this methodology were extensively described by Tschopp et al. (2015).

2.1.2. Continuum mechanics approach: field dislocation mechanics

We provide here a brief overview of the FDM model with the most important equations, more details about the model can be found in Acharya (2001). We consider the elastic deformation of a body containing dislocation lines. The presence of dislocations will be the source of elastic deformation and internal stresses. We first consider a general finite deformation setting and we then simplify into a small strain approximation. For simplicity, let us consider a body containing one dislocation line. The model begins by relating the incompatibility of the elastic transformation tensor to the Burgers vector. Let us consider two material configurations denoted as the reference configuration and the deformed configuration, distinguished by their position vectors \mathbf{X} and \mathbf{x} , respectively. The reference system corresponds to a continuous crystal (without cracks or voids) and without deformation. The deformed material configuration is obtained by applying to the reference configuration the transformation $\mathbf{F} = \partial \mathbf{x} / \partial \mathbf{X}$. The deformation gradient tensor \mathbf{F} is multiplicatively decomposed into plastic \mathbf{F}_p and an elastic \mathbf{F}_e tensors, $\mathbf{F} = \mathbf{F}_e \mathbf{F}_p$. Both tensors contain an incompatible non-gradient part, reflecting the elastic and plastic discontinuity due to a non-zero Burgers vector. A possible measure of this incompatibility is precisely the Burgers vector. The Burgers vector \mathbf{b} is defined as the integral of \mathbf{F}_e^{-1} along a closed circuit (C) around the dislocation line and is written as follows:

$$\mathbf{b} = - \oint_C \mathbf{F}_e^{-1} \cdot d\mathbf{x}. \quad (1)$$

In the above equation, the Burgers vector is measured in the intermediate, or plastic, configuration. If \mathbf{b} equals zero, it indicates compatibility of the elastic deformation. Conversely, when \mathbf{b} is non-zero, there is incompatibility. By applying Stokes' theorem to Eq. (1), we derive:

$$\mathbf{b} = - \iint_S \text{curl}(\mathbf{F}_e^{-1}) \cdot \mathbf{n} dS, \quad (2)$$

where S is the surface, with the unit normal \mathbf{n} , bounded by the Burgers circuit. From another point of view now, the Burgers vectors can be geometrically described through a second-order tensor known as the dislocation density tensor or so-called Nye tensor $\boldsymbol{\alpha}$ defined as (Nye, 1953):

$$\mathbf{b} = \iint_S \boldsymbol{\alpha} \cdot \mathbf{n} dS. \quad (3)$$

The tensor $\boldsymbol{\alpha}$ has components $\alpha_{ij} = b_i t_j$ in the Cartesian coordinate system, where the density b_i is the length of Burgers vector in direction i per unit surface and t_j is the unit dislocation line vector component in direction j . This means that the diagonal terms

Table 1

Elastic properties predicted for Tungsten with our DFT calculations and via EAM potential for copper. The elastic constants in tungsten were computed within a cell with 1 atom using a $34 \times 34 \times 34$ k-point mesh.

	C_{11} (GPa)	C_{12} (GPa)	C_{44} (GPa)
Tungsten	514.46	203.91	142.4
Copper	169.9	122.6	76.2

of the Nye tensor α represent screw dislocations whereas the non-diagonal terms represents edge dislocations. By identifying the two equations above, we obtain a non-integral expression that relates the inverse elastic transformation tensor to the Nye tensor:

$$\alpha = -\text{curl}(\mathbf{F}_e^{-1}). \quad (4)$$

In a small strain framework now, the inverse of the elastic transformation tensor \mathbf{F}_e^{-1} is related to the elastic distortion \mathbf{U}_e by $\mathbf{F}_e^{-1} = \mathbf{I} - \mathbf{U}_e$, where \mathbf{I} is the second-order identity tensor. The Eq. (4) can be rewritten as:

$$\alpha = \text{curl}(\mathbf{U}_e). \quad (5)$$

Following the work by Acharya (2001), we decompose the elastic distortion into an incompatible non-gradient, curl part \mathbf{U}_e^\perp , and a compatible, curl-free part \mathbf{U}_e^\parallel , which is a gradient. We therefore apply the Stokes Helmholtz decomposition:

$$\mathbf{U}_e = \mathbf{U}_e^\perp + \mathbf{U}_e^\parallel = \text{curl}\chi + \text{grad}\mathbf{w}. \quad (6)$$

By applying the **curl** operator to Eq. (6), we extract the incompatible elastic distortion, such that we have:

$$\alpha = \text{curl}(\mathbf{U}_e^\perp). \quad (7)$$

To obtain a unique and purely rotational solution to the above equation, we must also satisfy $\text{div} \mathbf{U}_e^\perp = 0$. By using the identity $\text{curl}(\text{curl} \mathbf{A}) = \text{grad}(\text{div} \mathbf{A}) - \text{div}(\text{grad} \mathbf{A})$, the incompatible elastic distortion is given as the solution of the following Poisson-type equation:

$$\text{div}(\text{grad} \mathbf{U}_e^\perp) = \Delta \mathbf{U}_e^\perp = -\text{curl}(\alpha). \quad (8)$$

Eq. (8) is solved through a computationally efficient numerical spectral method based on fast Fourier transform (FFT) algorithms, as detailed by Djaka et al. (2015). In order to know the total elastic distortion, we need to determine the compatible part, which serves to satisfy the stress equilibrium. Let us call \mathbf{T} the symmetric Cauchy stress tensor and \mathbf{C} the fourth order elasticity tensor. In the present study, we will use the elastic moduli obtained from Ab-initio simulations for the screw dislocation in tungsten, whereas for the GBs in copper, we employ the elastic constants predicted by the Mishin EAM potential (Mishin et al., 2001). The elastic constants were calculated in the standard basis of the BCC and FCC structures (see table 1). The stress tensor reads:

$$\mathbf{T} = \mathbf{C} : \mathbf{U}_e = \mathbf{C} : (\mathbf{U}_e^\perp + \mathbf{U}_e^\parallel). \quad (9)$$

and must satisfy the equilibrium equation $\text{div} \mathbf{T} = \mathbf{0}$ in the absence of inertia effects. Finally, using the definition of \mathbf{U}_e in Eq. (6), the stress equilibrium equation can be rewritten as:

$$\text{div}(\mathbf{C} : \text{grad}\mathbf{w}) + \mathbf{f}^\perp = \mathbf{0}, \quad (10)$$

where $\mathbf{f}^\perp = \text{div}(\mathbf{C} : \mathbf{U}_e^\perp)$ can be interpreted as a volumetric force resulting from the elastic incompatibility associated with dislocations. The Eq. (10) is also approximated through a computationally efficient scheme based on FFT algorithms in the framework of heterogeneous elasticity (Djaka et al., 2015).

2.2. Atomistic to continuum mechanics transfer methods

2.2.1. Hartley and Mishin original algorithm

In this section, we adopt the approach introduced by Hartley and Mishin (2005) to calculate the Nye tensor α per atom. The Nye tensor can be expressed as the curl of lattice correspondence tensor \mathbf{G} , which is the inverse elastic transformation that maps the position vectors of atoms in a deformed crystal configuration \mathbf{dx} onto those of a perfect reference crystal configuration \mathbf{dX} by the equation:

$$\mathbf{dX} = \mathbf{G} \cdot \mathbf{dx}. \quad (11)$$

To compute the lattice correspondence tensor \mathbf{G} , we define $\mathbf{P}^\gamma (\gamma = \{1, 2, 3, \dots, n\})$ and $\mathbf{Q}^\beta (\beta = \{1, 2, 3, \dots, m\})$ as the set of position vectors between atom i and all its neighboring atoms (n and m) within a specified cutoff radius R_c in the perfect configuration and the deformed configuration respectively. It is important to note that the choice of cutoff radius significantly impacts the \mathbf{G} fields and the Burgers vector calculations. In the systems simulated here, we select a cutoff distance of $R_c = 0.93a_0$ and $0.86a_0$ for BCC and FCC, respectively. These values correspond to half the distance between the first and second neighbor shells in the BCC and

FCC systems. For each \mathbf{Q}^β we locate the corresponding \mathbf{P}^γ with the closest angle match. This is achieved by calculating the angular difference between the two vectors, i.e., for each \mathbf{Q}^β we seek the \mathbf{P}^γ vector yielding the shortest angle. If there is no \mathbf{P}^γ vector found within a fixed tolerance θ_{max} , we exclude that \mathbf{Q}^β . However, if a match is found, we compare the lengths of the two \mathbf{Q}^β vectors and retain the one that is closest in length to \mathbf{P}^γ . According to Hartley and Mishin (2005) suggestion, we employed $\theta_{max} = 43^\circ$ for BCC and $\theta_{max} = 27^\circ$ for FCC systems, which closely aligns with half of the angle between the \mathbf{P}^γ vectors. After the vector rejections, the number of \mathbf{P}^δ and \mathbf{Q}^δ sets, with $\delta = \{1, 2, \dots, s\}$, will be either equal to or less than β and γ . The lattice correspondence tensor \mathbf{G} is evaluated for a given atom as a least squares solution of the linear matrix equation:

$$\mathbf{Q} \cdot \mathbf{G} = \mathbf{P}, \quad (12)$$

where matrices \mathbf{P} and \mathbf{Q} have dimensions of $(s \times 3)$, with each row representing the index of vector (δ) and each column representing the components of the vectors along the reference Cartesian axes. According to Harley and Mishin convention, the Nye tensor α can be expressed as function of the lattice correspondence tensor \mathbf{G} by:

$$\alpha = -\text{curl}(\mathbf{G}). \quad (13)$$

It is important to highlight that within the Hartley and Mishin approach, the counterpart to the lattice correspondence tensor is represented as the transpose of the elastic transformation inverse in the FDM approach. This means that:

$$\mathbf{G} = (\mathbf{F}_e^{-1})^T. \quad (14)$$

By using the Einstein notation, the Nye tensor in our FDM model is thus expressed in rectangular cartesian components as:

$$\alpha_{ij} = -e_{jkl} \frac{\partial G_{il}^T}{\partial x_k}, \quad (15)$$

where \mathbf{e} is the Levi-Civita permutation tensor. In the Hartley and Mishin algorithm, the per-atom Nye tensor is then estimated through an approximation of spatial derivatives involved in the curl operation. The algorithm has been recently implemented in available atomistic tools designed for the construction and analysis of large-scale atomic systems, such as Anon (2023) and Hirel (2015). Both tools were tested and yielded similar results for the \mathbf{G} and α per-atom fields. Notably, the simulation time needed is a few seconds.

2.2.2. Atomistic to continuum transfer

In this section, we outline two different approaches employed for using possible atomistic data for a given crystal defect (dislocations or GBs), as input in the FDM model. We remind that the FDM field Eqs. (8) and (10) are numerically approximated on a regular FFT grid, following Djaka et al. (2015). As such, we need to transfer per-atom atomistic (ab-initio or MS) data onto an FFT grid. Atomistic, per-atom data fields, can be either \mathbf{G} or directly α . As illustrated in Fig. 1, the first approach, denoted \mathbf{G} method, involves the computation of the per-atom lattice correspondence tensor using the Hartley and Mishin algorithm (Fig. 1b). The tensor components are then interpolated onto the FFT grid (Fig. 1c), on which we can then estimate the curl to determine the Nye tensor using a finite difference approximation (Fig. 1d). From this, we can solve the FDM equations to obtain the continuous elastic distortion field Fig. 1e. The second approach, denoted α method, involves the calculation of the per-atom Nye tensor using the Hartley and Mishin algorithm (Fig. 1f). The components α_{ij} of this tensor are then directly interpolated on the FFT grid (Fig. 1g) and use as input to solve the FDM equations, leading to another continuous elastic distortion field (Fig. 1h). Finally, we can compare the continuous elastic distortion fields obtained via both \mathbf{G} and α methods to the elastic per-atom elastic fields obtained using the Hartley and Mishin algorithm. It is worth noting that we evaluated various interpolation methods, including spline, cubic, and nearest neighbor interpolations. It appeared that linear interpolation was perfectly adequate (see Figures S5 and S6 in Supplementary Material). In terms of computation time the transfer method, including interpolation and the resolution of the Field dislocation mechanics (FDM) equations, is not computationally expensive. The simulation time is a few seconds on one processor. However, it is important to note that the atomistic simulations remain computationally expensive. We have provided a detailed table in the supplementary material, showing the simulation time and the number of CPUs required for each defect and for each Fast Fourier Transform (FFT) grid resolution. It is thus computationally very cheap to build an entire database of defects, providing the atomistic configurations of defects are already available and a fully automated framework has been designed. As an example of such available data, the grain boundaries dataset from Tschopp et al. (2015)

3. Results and discussion

3.1. Benchmark test

The transfer methods introduced in Section 2.2.2 are first assessed by considering $1/2[111]$ screw dislocations in tungsten. Fig. 2 depicts the influence of FFT grid resolution on the Nye component α_{33} distribution using \mathbf{G} and α methods. For the finest resolution tested (0.5 Å, Fig. 2(b) and (c)), both methods successfully capture the screw density distribution obtained with DFT (Fig. 2(a)). However, the three-fold symmetry of the screw dislocation core is only captured by the \mathbf{G} method at 0.5 Å resolution (Fig. 2(b)). It is also with this method and resolution that we manage to obtain the most compact core, which is a specific feature of screw dislocation cores in BCC metals. Fig. 2(c) and (e) show that a 2 Å resolution does not reproduce the 3-fold symmetry of the dislocation core, for either method. We have quantitatively evaluated both methods by calculating the error on the magnitude of the Burgers vector

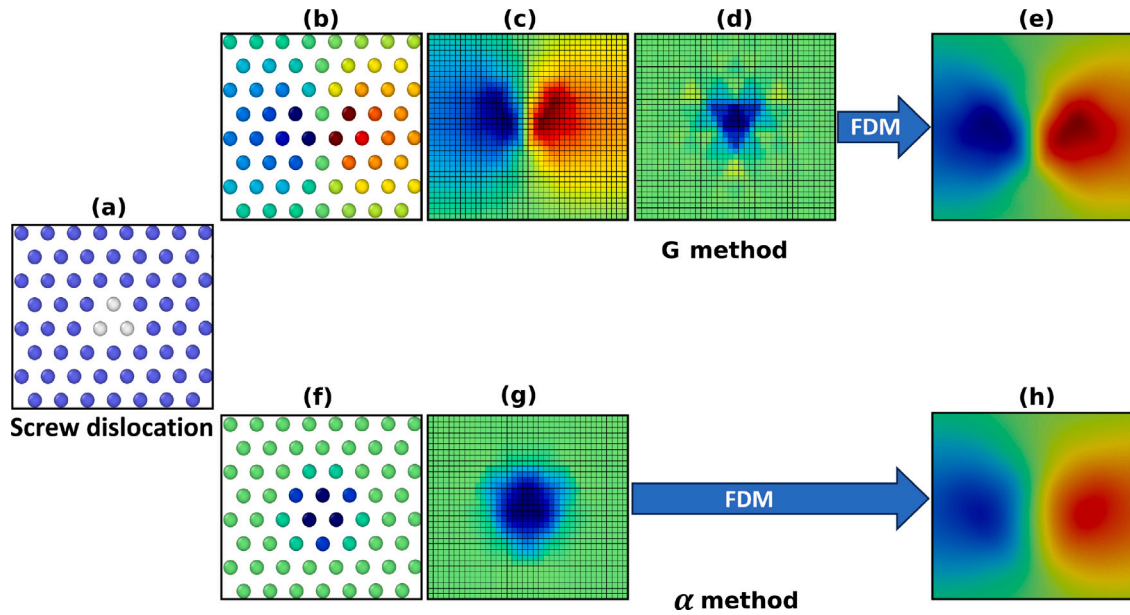


Fig. 1. Schematic representation of the atomistic to continuum transfer techniques: (a) Visualization of a $1/2[111]$ tungsten screw dislocation core in OVITO (Stukowski, 2009). The atomistic core structure is colored using common neighbor analysis: Blue atoms represent BCC environment and white atoms indicate a non-BCC environment. The figures (b), (c), (d) and (e) depict the workflow of the G method. (b) The component G_{23} of the per-atom lattice correspondence tensor calculated by Harley and Mishin algorithm. (c) Interpolation G_{23} on the FFT grid. (d) Calculation of the component a_{33} of the Nye tensor on the FFT grid. (e) Visualization of elastic distortion maps obtained from solving the FDM equations. The figures (f),(g) and (h) represent the workflow of the α method. (f) The component a_{33} of the per-atom Nye tensor calculated by Harley and Mishin algorithm. (g) Interpolation of a_{33} on the FFT grid. (h) Visualization of elastic distortion maps obtained from solving the FDM equations. (For interpretation of the references to color in this figure legend, the reader is referred to the web version of this article.)

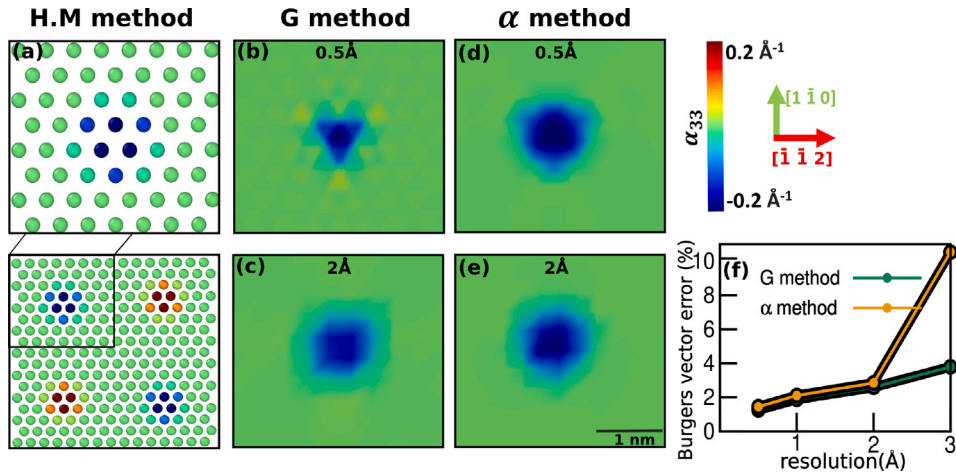


Fig. 2. Screw dislocations in tungsten. Effect of FFT grid resolution on Nye dislocation density distributions and Burgers Vector norm error using G and α methods. (a) Visualization of the per-atom component a_{33} of the Nye tensor as obtained from the Hartley-Mishin method applied to the DFT calculations. Red represents positive dislocation density and blue the negative one. (b) and (c): maps illustrating the screw dislocation density distribution obtained using the G method with FFT grid resolutions of 0.5 \AA and 2 \AA , respectively. (d) and (e) depict screw dislocation density distributions using the α method with 0.5 \AA and 2 \AA FFT grid resolutions. (f) The variation of the Burgers vector norm error as a function of the grid resolution using the G method (green line) and α method (yellow line). (For interpretation of the references to color in this figure legend, the reader is referred to the web version of this article.)

relative to the ideal value ($b_{ideal} = 2.762 \text{ \AA}$). Given the Nye tensor definition in Eq. (3), the Burgers vector is numerically calculated by integrating the Nye tensor over a rectangular grid in a plane normal to the dislocation line. Fig. 2(f) depicts the variation of the error as a function of the FFT grid resolution for both methods.

We observe two distinct regions in Fig. 2(f). For resolutions up to 2 \AA , both methods exhibit similar efficiency, while for resolutions higher than 2 \AA , the α method shows noticeable increase in the error percentage. This correlates with the fact that

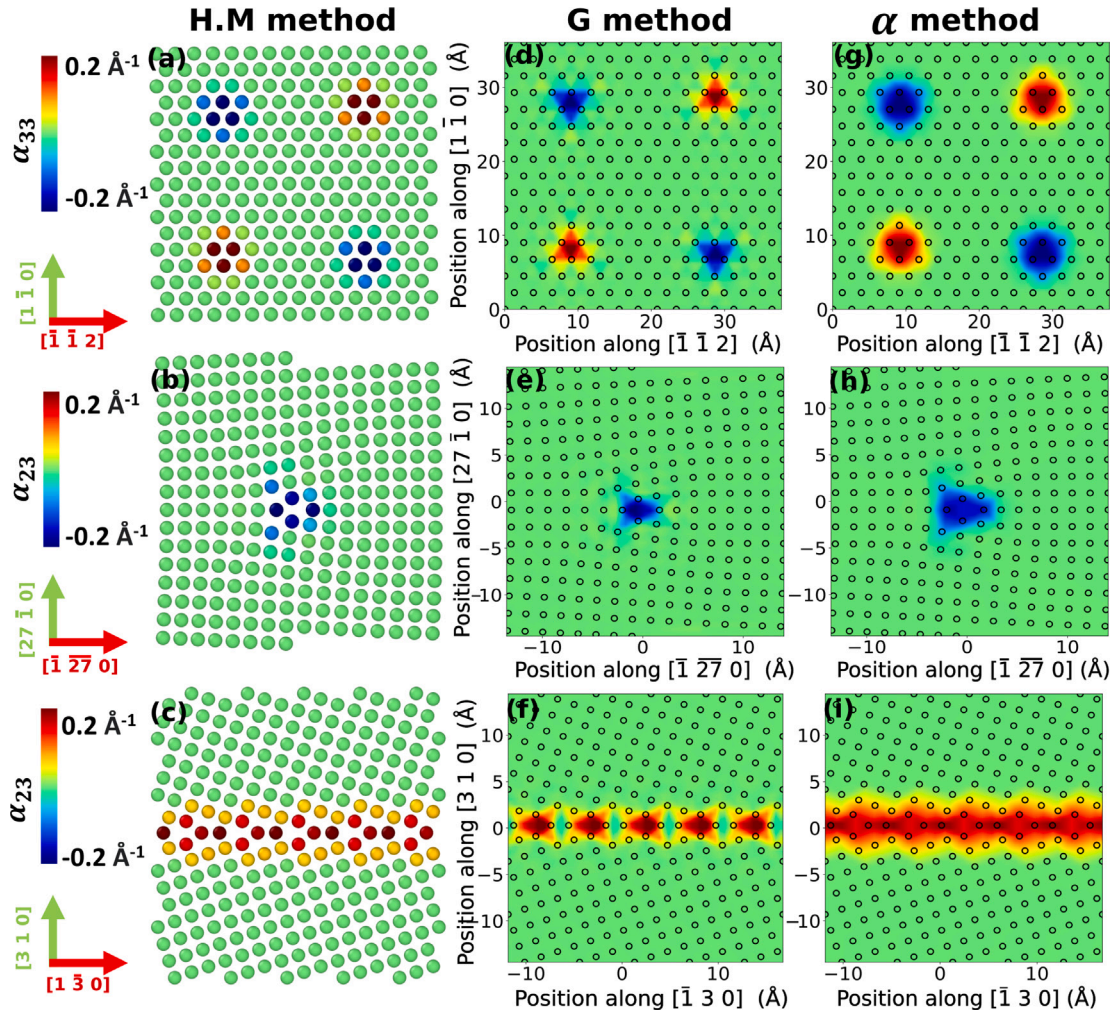


Fig. 3. Comparison of Nye dislocation density distributions obtained with the G and α transfer methods using a 0.5 Å FFT grid resolution. (a), (b) and (c) Visualization of the component α_{33} and α_{23} of the Nye tensor for the screw dislocation quadruple in tungsten, structural units within LAGB and HAGB in copper respectively after atomistic relaxation. (d), (e) and (f) Represent maps displaying the screw and edge dislocation densities obtained via the G method. (g), (h) and (i) show the same densities obtained with the α method.

the core is less compact than expected for higher resolutions. Thereby, when using coarser resolutions, the accurate description of the core is compromised due to the loss of information during interpolation. An identical procedure was carried out for edge dislocations within LAGB in copper (see Figure S3 in Supplementary Material) and also showed an increased error percentage for resolutions higher than 0.5 Å, and a loss of core symmetry for resolutions of 2 Å and more. Consequently, in the following, we consider the resolution of 0.5 Å, which provides the best description of the dislocation core.

3.2. Inspection of Nye dislocation density distributions

In the following, we compare qualitatively the efficiency of the G and the α methods in terms of Nye dislocation density distributions for the $1/2[111]$ screw dislocations in tungsten (screw densities), LAGB and HAGB in copper (edge densities). The first column of Fig. 3 shows the distribution of the atomic Nye tensor for the three defects studied. Hartley and Mishin's method can be extended to calculate the Nye tensor within a grain boundary. This is particularly useful because identifying the ideal reference configuration can be challenging for systems as complex as grain boundaries, such as multi-phase boundaries. In this study, we opted for the Displacement Shift Complete (DSC) lattice as our reference system for the grain boundary (Grimmer, 1974), as it is typically closely aligned with the positions of the atoms within the GB (Winter et al., 2022). In the third row, we examine the atomic Nye tensor of a symmetric tilt HAGB $\Sigma 5(310)[001]$ (Figs. 3(c), Fig. 3(f) and Fig. 3(i)). This specific system holds considerable importance to assess our approach as the GB structure is not described by a dislocation array as for LAGB, but by structural units. We observe that for all defects, the G method results in a highly concentrated Nye edge dislocation density distribution in each

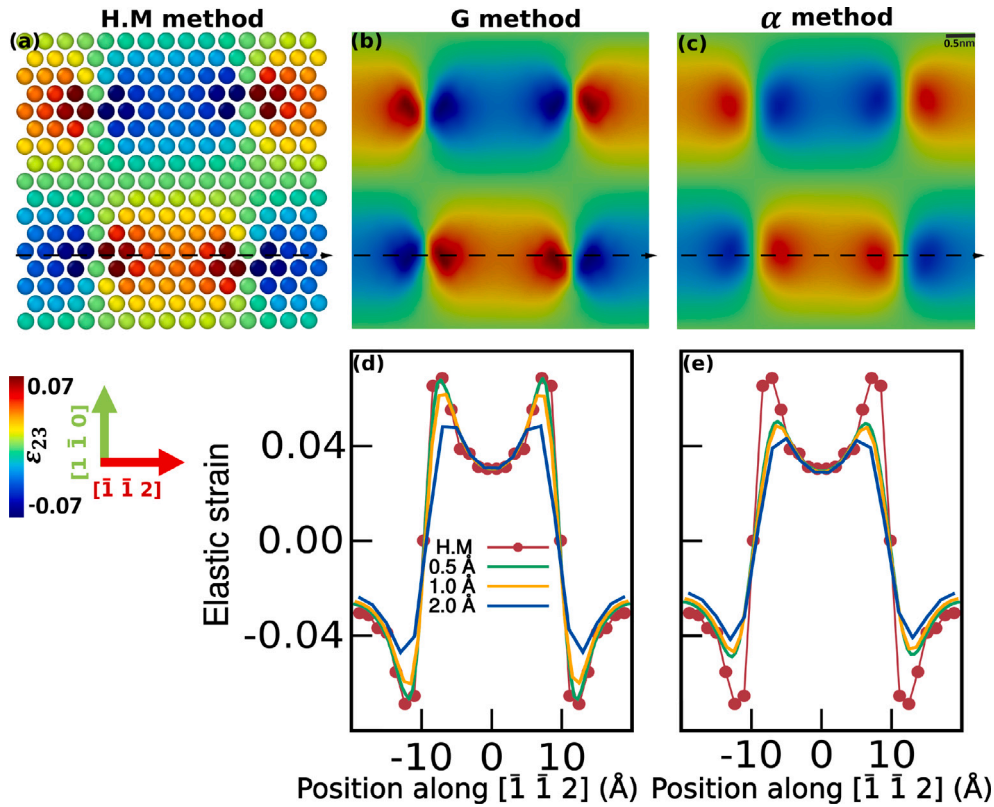


Fig. 4. Elastic strain field obtained for screw dislocation quadruple in tungsten with the G and α transfer methods using a 0.5 Å FFT grid resolution and compared to the HM method atomistic result. (a) Visualization of the per-atom strains ε_{23} using Hartley and Mishin method. (b) and (c) Maps displaying the elastic strain fields obtained via the G and α methods. The dashed lines indicate the directions for plotting profiles. (d) and (e) represent the elastic strain ε_{23} profiles along the $[\bar{1} \bar{1} 2]$ direction obtained with the G and α methods.

structural unit, whereas the α method produces a spread-out distribution. Interestingly, the result from the G method for LABG and HAGB suggests that each structural unit can be interpreted as an edge dislocation with an equivalent Burgers vector $[0 1 0]$. While dislocation based models are usually said to be limited to low misorientations ($< 15^\circ$), our results rather suggest they are actually also applicable to HAGBs. Last but not least with the G method, the edge dislocation core in the LABG and the structural unit cores in the HAGB have the largest edge dislocation density at the place where there is no atom (where there is an excess volume). As such, the G method offers a more appropriate continuous description of the defect cores than the per-atom Nye estimation for such defects. However, we expect certain limitations of the proposed method when dealing with highly disordered grain boundaries where structural units are indiscernible.

3.3. Inspection of elastic fields: strain and rotation

We will now explore the applicability of the transfer methods in evaluating the elastic strain/rotation fields generated by the dislocations and GBs. First, the atomic elastic strain field obtained through the lattice correspondence tensor will be qualitatively compared to the continuous elastic fields obtained from FDM simulations, using input dislocation densities from the transfer methods. The components of the per-atom strain ε_{ij} can be computed from the lattice correspondence tensor \mathbf{G} by

$$\varepsilon_{ij} = ((\delta_{ij} - G_{ij}) + (\delta_{ji} - G_{ji}))/2, \quad (16)$$

where δ_{ij} is the Kronecker symbol. The Figs. 4 (a), 4(b) and 4(c) represent the distribution of the out-of-plane shear component ε_{23} of the elastic strain field from a screw dislocations in tungsten. The color scale used in Fig. 4 represents strain ranging from -7% to $+7\%$. It is identical for both atomistic and continuous representations.

In the case of positive screw dislocations, there is positive shear strain on the left side and a negative shear strain on the right side of the dislocation core, which qualitatively aligns with the elastic field predicted for a straight screw dislocation line in isotropic elasticity. As described earlier, the structural units composing the low-angle grain boundary can be seen as an array of edge dislocations. Figs. 5 (a), 5(b) and 5(c) exhibit the distribution of the in-plane shear component ε_{12} of the elastic strain field of an isolated dislocation in the LABG. The field acquired by both transfer methods closely aligns with the results from atomistic

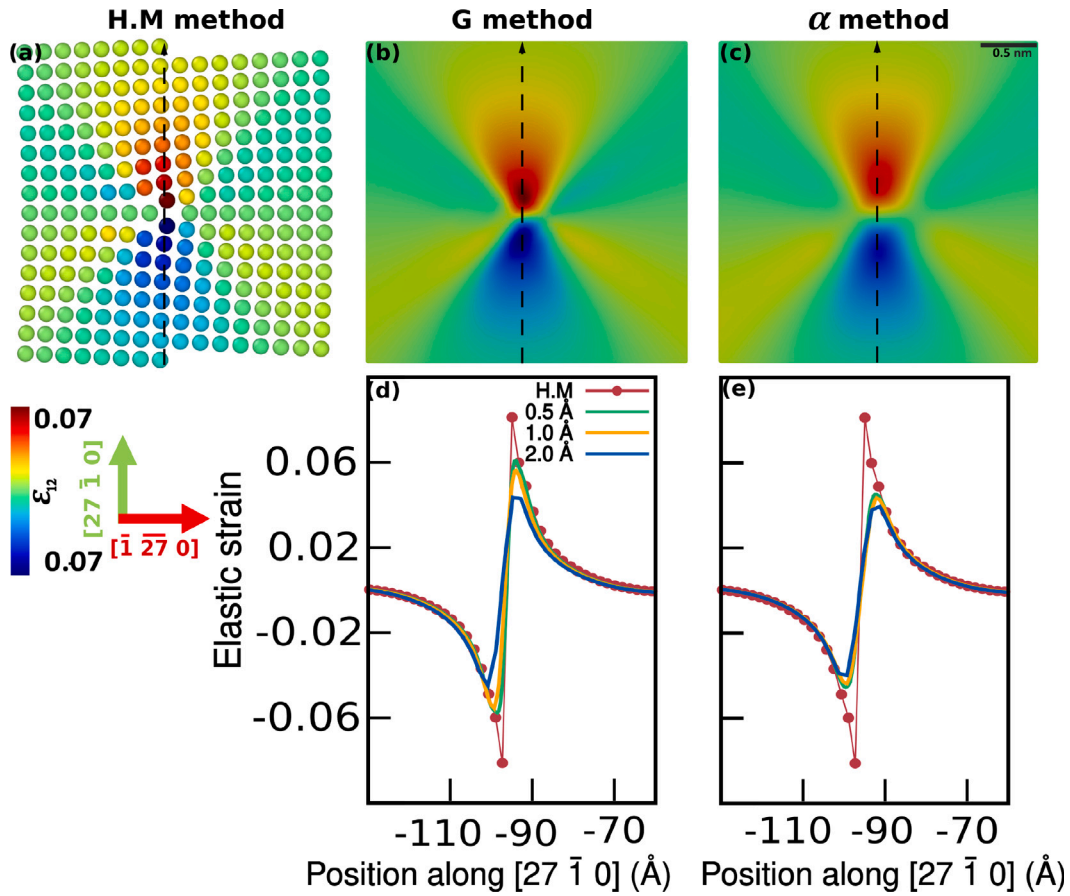


Fig. 5. LAGB in copper: Elastic strain field obtained with the G and α transfer methods using a 0.5 Å FFT grid resolution and compared to the HM method atomistic result. (a) Visualization of the per-atom elastic strain ε_{23} . (b) and (c) Maps displaying the elastic strain field ε_{23} obtained via the G and α methods. The dashed lines indicate the directions for plotting profiles. (d) and (e) represent the elastic strain ε_{12} profiles along the $[27 \bar{1} 0]$ direction obtained with the G and α methods.

calculations, demonstrating a good agreement between both approaches. In the case of the screw dislocations and LAGB however, we observe that the G method much better captures the high strain gradients in the immediate core region of defects, while both methods accurately capture the relatively smaller strains in regions away from the defect cores.

To quantify these observations, we plot the distribution profiles of the elastic fields ε_{23} and ε_{12} , following the directions marked with dashed lines on Figs. 4 and 5(d). For the screw dislocation cores, Figs. 4 (d) and 4(e) compare the profiles of the atomic strain field (red solid line with symbols) and the continuous strain fields (solid lines) obtained using the G and α methods respectively, for different FFT grid resolutions. The results show the correct reproduction of the significant gradient of strain at dislocations core, with the G method and fine resolutions. The ability to capture these core-level strains is degraded at a resolution of 2 Å. The comparison between the atomistic and the continuous strain field obtained using the α method reveals that this approach is not as effective as the G method in capturing the high strain levels near the dislocation core, even when employing the finest resolution. It is also noteworthy that the resolution has more effect on the G method than on the α method, and that both methods capture correctly the long-range elastic fields away from the defect cores, whatever the resolution. Similar findings apply to the case of the LAGB (Figs. 5 (d) and 5(e)). While the G method reproduces almost perfectly the strain fields at the core of screw dislocations obtained from DFT, it is slightly less efficient to reproduce the elastic fields observed around the dislocation and structural unit cores within grain boundaries as obtained with semi-empirical potentials. Figs. 6 (d) and 6(e) show the profiles of the tilt elastic rotation field, describing the grain boundary misorientation angle along the $[3 \bar{1} 0]$ direction, using the G and α methods, respectively. Both methods effectively capture the expected rotation field, the G method providing a slightly better agreement with atomistic results. For the finest FFT grid resolution, both approaches converge to a misorientation angle of 0.632 radians, corresponding to the characteristic misorientation of the $\Sigma 5(310)[001]$ grain boundary considered in this work.

3.4. Application to dislocation/grain boundary interactions

In light of the previous examples, the G method, using a 0.5 Å FFT resolution, demonstrates to be effective in capturing the short and long range mechanical fields generated by screw dislocations, low and high angle grain boundaries. The next focus involves the

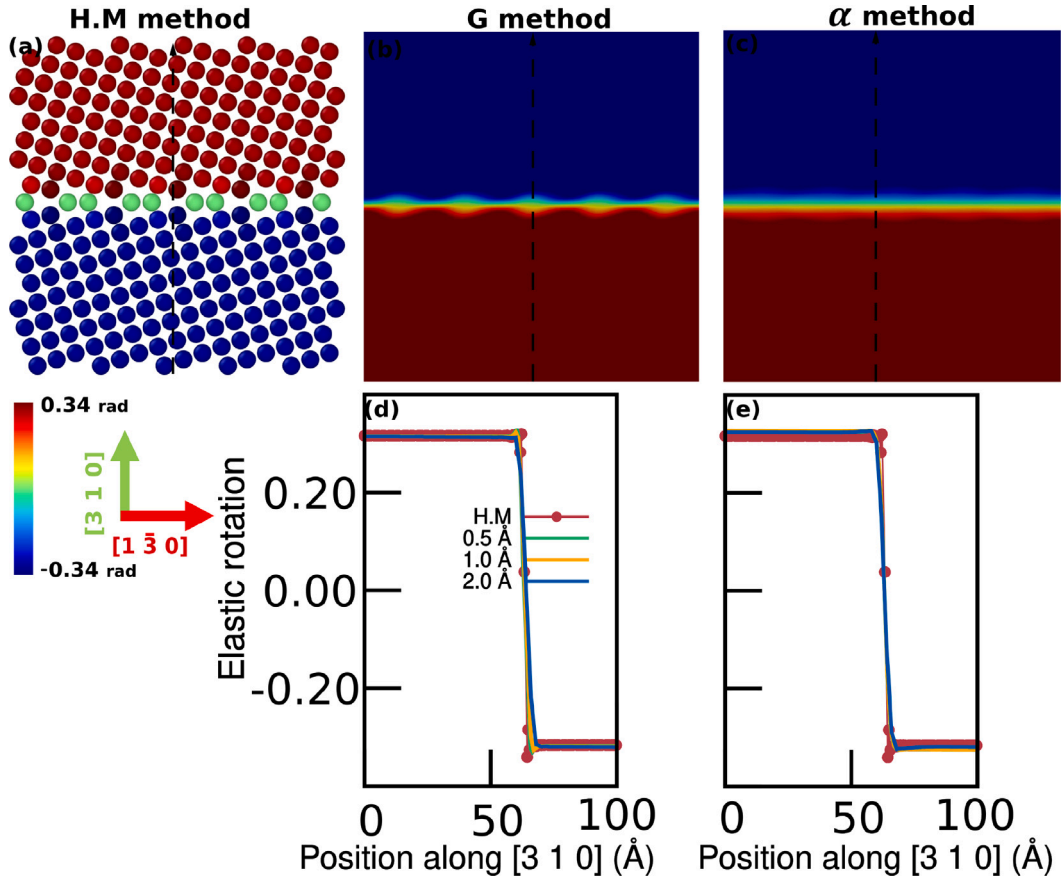


Fig. 6. HAGB in copper: Elastic rotation field obtained with the G and α transfer methods using a 0.5 Å FFT grid resolution and compared to the HM method. (a) Visualization of the per-atom elastic rotation. (b) and (c) Maps displaying the rotation field obtained via the G and α methods. The dashed lines indicate the directions for plotting profiles. (d) and (e) represent the tilt rotation profiles along the $[3\ 1\ 0]$ direction obtained with the G and α methods.

application of the G method to investigate the elastic interactions between $\Sigma 291(13\bar{1}1)[\bar{1}\bar{1}2]$ symmetric tilt grain boundary and edge extrinsic dislocations in copper. Two molecular static simulation scenarios were performed. In the first scenario (Fig. 7(a)), the extrinsic dislocation is aligned with an intrinsic dislocation composing the grain boundary. The two dislocations have opposite sign. In the second scenario (Fig. 7(d)), the dislocation is shifted by two $\{111\}$ planes in such a way that the extrinsic dislocation is aligned in between two intrinsic dislocation composing the grain boundary. To bring the systems into equilibrium, the FIRE algorithm (Guénolé et al., 2020) is used and the configurations were considered optimized when the norm of the global force vector is below 10^{-6} eV/Å.

During the minimization process, the extrinsic edge dislocations are dissociated into two Shockley partials. This is illustrated in Figs. 7 (a) and 7(d), where two positive Nye distributions can be seen separated by a specific distance corresponding to the stacking fault separating the two Shockley partials. Figure S4 (in supplementary materials) describes the details of the systems' configuration using the per-atom Nye dislocation density. The Burgers vector norm of dislocations is $b = 2.56$ Å. This value is calculated by integrating the Nye tensor over a rectangular grid in a plane normal to the dislocation line. The G method is applied to capture the interactions of the elastic stress fields induced by the inserted edge dislocation and the low angle grain boundary, and compared to the virial stress calculated by molecular static simulations. Depending on the initial position of the extrinsic dislocation, two distinct interaction scenarios are observed. Figs. 7 (b) and (c) depict the per-atom virial shear stress and that obtained with the G transfer method, respectively, illustrating the first interaction scenario. The extrinsic edge dislocation has annihilated with one intrinsic dislocation composing the GB. The grain boundary is indeed described as an array of edge dislocations, where the core of each dislocation undergoes slight dissociation into two Shockley partials. This annihilation results in a local increase in the stress field due to a reduction in the elastic screening between neighboring intrinsic GB dislocations. In the second scenario, the extrinsic dislocation stabilizes near the grain boundary, causing disruption in the dislocation network within the grain boundary and slight migration towards the dislocation (Figs. 7 (e) and (f)). The short-range elastic interactions between the extrinsic dislocation and the GB dislocations is rather well captured by the G method in both scenarios. Note that this relaxed configuration is not realistic, as annihilation should likely occur by local climb process. It is not possible here as simulations are performed at 0K. Similarly, we evaluated the interaction between an extrinsic edge dislocation and a $\Sigma 35(5\bar{3}1)[1\bar{1}2]$ 34.05° high angle grain boundary in copper.

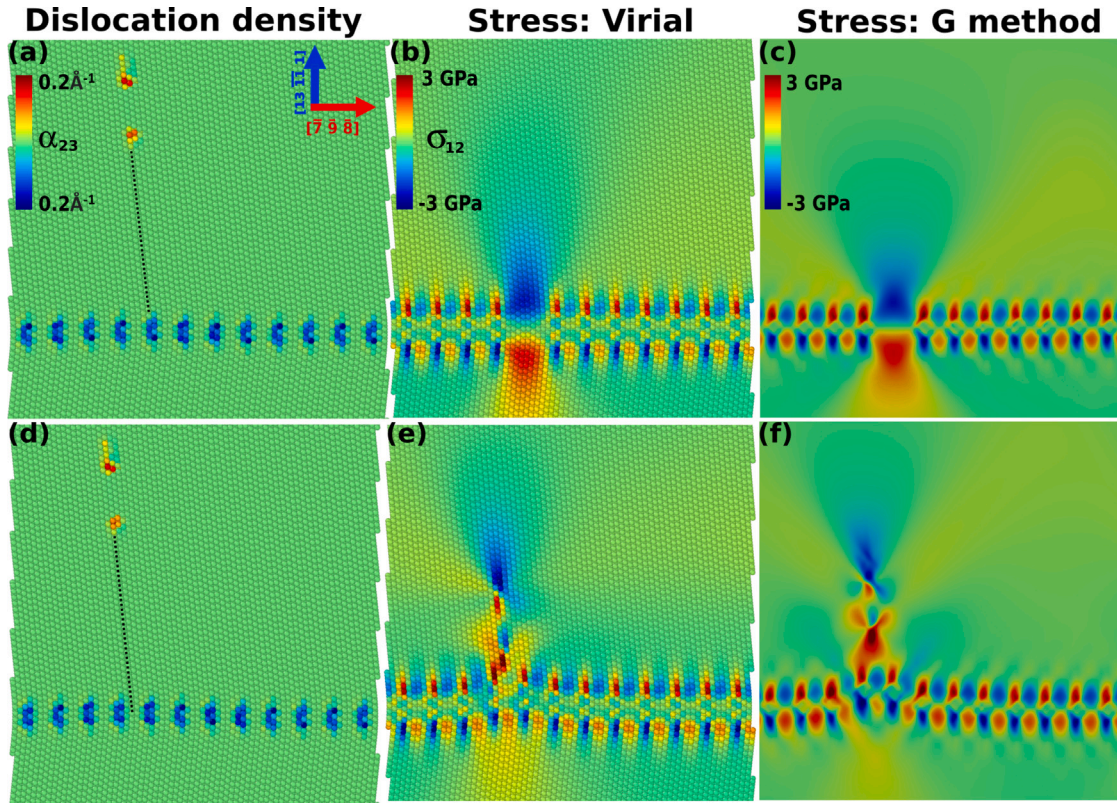


Fig. 7. Interaction between an extrinsic edge dislocation and a $\Sigma 291(13\bar{1}11)[\bar{1}\bar{1}2]$ low angle STGB in copper, with two scenarios: the edge dislocation will annihilate with one composing the GB (a, b, c); the edge dislocation will stop nearby the GB (d, e, f). Figures (a, d) show the per-atom Nye dislocation density α_{23} in the initial (unrelaxed) configuration for both scenarios. The presence of two positive α_{23} distributions indicates a dissociation of the extrinsic dislocation into Shockley partials. The dashed black lines indicate the $\{111\}$ glide plane of the extrinsic edge dislocation. In (b, e) is shown the per-atom virial stress σ_{12} of the final (relaxed) configuration, when the edge dislocation has interacted with the GB, for both scenarios. Figures (c, e) show the same stress fields obtained via application of the G method with a 0.5 \AA FFT grid resolution.

The structural units forming the grain boundary, as depicted in Figure S7 (Supplementary Material), are represented by an edge dislocation with highly localized elastic strain fields. Figure S7 (Supplementary Material) compares the stress field obtained by the G method with the Virial stress. We observed that after energy minimization, the edge dislocations glide and stop nearby the grain boundaries, affecting their elastic fields. However, no real interactions (such as dislocation absorption and decomposition) are predicted by this simulation, which somehow resembles that of the low angle grain boundary. To predict more complex interactions, one would need to test other configurations, run simulations with finite temperature and/or applied stress.

4. Conclusions and perspectives

This paper introduces a new methodology to establish an atomistic to continuum mechanics crossover method, whereby atomic positions in defected regions are used to derive a continuous Nye dislocation density field that is an input in a Field Dislocation Mechanics model. This approach is primarily based on the derivation of the per-atom Nye and lattice correspondence tensors obtained from the Hartley and Mishin method, which we then use as possible inputs on a FFT grid to derive as best as possible the continuous Nye tensor for FDM simulations. The practical outcomes of our research underline the effectiveness of the G method, which relies on interpolating the components of the lattice correspondence tensor as input on the FFT grid. With this method, the FDM model can accurately predict the Burgers vector of defects, as well as the elastic strain and rotation fields near and away from the defect cores, in particular in the case of the screw dislocations simulated by DFT. Note also the efficiency of the FDM model, despite it being formulated within a small strain, linear elastic framework. Another interesting and unexpected result for high angle grain boundaries with structural units closely packed, is that the latter can be described as localized, equivalent, edge dislocations. This approach is thus in favor of dislocation based models for GBs and represents a compelling alternative for modeling high angle grain boundaries without relying on disclination fields (Fressengeas et al., 2014). The methodology was extended to investigate the interactive elastic fields between an extrinsic edge dislocations and a low angle grain boundary. It highlights how the stress field due to the presence of the dislocation influences the dislocation network at the grain boundary. We have also tried to simulate a more complex case involving the interaction between edge dislocations and a high-angle tilt grain boundary.

Based on our examination of FFT Field Dislocation Mechanics simulations incorporating atomistically informed input dislocation density, we conclude that one major implication of the present work is the following. The per-atom lattice correspondence tensor G is well estimated using the Hartley & Mishin algorithm, which well conserves the incompatibility of G . Such is achieved by directly expressing G as the matrix that maps vectors from the deformed atomic configuration onto the reference configuration. In contrast, extracting atomic displacement fields and then taking their spatial gradients to derive G would lead to a curl-free gradient tensor G , and one would completely lose the incompatibility of G and predict a null dislocation density. By comparing our method “alpha”, where we directly interpolate the per-atom dislocation density, to the “ G ” method, where we interpolate the per-atom G tensor and then derive the dislocation density with finite differences on a regular grid, we show however that the per-atom Nye dislocation density is less efficiently captured by the Hartley & Mishin algorithm. There are two reasons for this. First, 3D spatial derivatives in the Cartesian frame are not accurately estimated using atomic values and positions. Second and perhaps more importantly, large local dislocation densities in the core regions of defects can be missed because there is no atom in such regions to bear the corresponding dislocation density. This second problem is indeed observed in structural units in our work, where the G -method shows that the largest dislocation density is located at the center of structural units, which contain no atom. As part of the dislocation density is missed, the predicted elastic fields by FDM do not match those from atomistics. The present results thus suggest that the per-atom G tensor is well estimated by the Hartley & Mishin algorithm, but that it is preferable to then derive the dislocation density by interpolating the G tensor on a regular grid. This appears to be true for all benchmark cases studied in this work.

A development of our transfer approach could be on polycrystalline materials. While we considered here only (quasi) 2D configurations, our method is intrinsically 3D and can be extended to study interfacial plasticity, i.e., mechanisms related to grain boundary - dislocation interactions. This would allow considering the presence of initial grain boundary dislocation content and short/long range internal stresses, and the effects on the development of plastic deformation within grains and at/across GBs. An ongoing development of our approach concerns the assessment of strain gradient plasticity models based on GND or Nye dislocation density tensor. Such models add supplementary internal energy functionals based on the Nye tensor to better capture size effects (Forest and Guéninchault, 2013) or dislocation transfer mechanisms at GBs (Jebahi et al., 2020), for instance. By applying our method to excess grain boundary energies measured by atomistic simulations for various grain boundaries, it is possible to test different energy functionals proposed in the literature and to quantify the internal characteristic lengths introduced. Furthermore, ongoing efforts are directed towards extending the applicability of our workflow to hexagonal close-packed (HCP) materials.

While the method we propose here holds great potential for various defects and structures, we recognize that computing the per-atom Nye tensor may pose challenges in specific cases, particularly with complex structures like phase boundaries or crystal defects in chemically complex materials such as high entropy alloys. Furthermore, the method may encounter limitations when applied to highly disordered grain boundaries, which does not exhibit well defined structural units. Future work may focus on exploring these corner cases and other extensions of the approach, including taking into account dynamic effects.

CRediT authorship contribution statement

Houssam Kharouji: Methodology, Software, Validation, Formal analysis, Investigation, Writing – original draft, Visualization. **Lucile Dezerald:** Conceptualization, Methodology, Writing – review & editing, Supervision. **Pierre Hirel:** Methodology, Software, Writing – review & editing, Supervision. **Philippe Carrez:** Writing – review & editing, Supervision. **Patrick Cordier:** Writing – review & editing. **Vincent Taupin:** Conceptualization, Methodology, Formal analysis, Software, Writing – original draft, Supervision. **Julien Guérolé:** Conceptualization, Methodology, Writing – original draft, Supervision, Project administration, Funding acquisition.

Declaration of competing interest

The authors declare no conflicts of interest.

Data availability

Data will be made available on request.

Acknowledgments

H.K., L.D., V.T. and J.G. acknowledge funding from the LabEx DAMAS (Laboratory of Excellence on Design of Alloy Metals for low-mAss Structures). H.K. acknowledges financial support from the Région Grand-Est. V.T., L. D. and J.G. acknowledges funding from the French National Research Agency (ANR), Grant ANR-21-CE08-0001 (ATOUM). High Performance Computing resources were provided by the EXPLOR center of the Université de Lorraine and by the GENCI-TGCC (grant Grant 2022-A0120911390). P.H., Ph.C. and P.C. acknowledge funding from the European Research Council (ERC) under the European Union’s Horizon 2020 research and innovation programme under grant agreement No 787198 – TimeMan.

Appendix A. Supplementary data

Supplementary material related to this article can be found online at <https://doi.org/10.1016/j.ijplas.2024.103990>.

References

- Acharya, A., 2001. A model of crystal plasticity based on the theory of continuously distributed dislocations. *J. Mech. Phys. Solids* 49.
- Anon, 2023. Atomistic manipulation toolkit. <https://www.ctcms.nist.gov/potentials/atomman>.
- Berbenni, S., Paliwal, B., Cherkaoui, M., 2013. A micromechanics-based model for shear-coupled grain boundary migration in bicrystals. *Int. J. Plast.* 44.
- Berbenni, S., Taupin, V., Djaka, K.S., Fressengeas, C., 2014. A numerical spectral approach for solving elasto-static field dislocation and g-disclination mechanics. *Int. J. Solids Struct.* 51.
- Berry, J., Provatas, N., Rottler, J., Sinclair, C.W., 2014. Phase field crystal modeling as a unified atomistic approach to defect dynamics. *Phys. Rev. B* 89.
- Bertin, N., Sills, R.B., Cai, W., 2020. Frontiers in the simulation of dislocations. *Annu. Rev. Mater. Res.* 50, 437–464.
- Beyerlein, I., Hunter, A., 2016. Understanding dislocation mechanics at the mesoscale using phase field dislocation dynamics. *Phil. Trans. R. Soc. A* 374.
- Bienvenu, B., Dezerald, L., Rodney, D., Clouet, E., 2022. Ab initio informed yield criterion across body-centered cubic transition metals. *Acta Mater.* 236.
- Bienvenu, B., Fu, C.C., Clouet, E., 2020. Impact of magnetism on screw dislocations in body-centered cubic chromium. *Acta Mater.* 200, 570–580.
- Borodin, E., Mayer, A., Gutkin, M.Y., 2020. Coupled model for grain rotation, dislocation plasticity and grain boundary sliding in fine-grained solids. *Int. J. Plast.* 134.
- Clouet, E., Bienvenu, B., Dezerald, L., Rodney, D., 2021. Screw dislocations in BCC transition metals: from ab initio modeling to yield criterion. *C.R. Phys.* 22.
- Djaka, K., Taupin, V., Berbenni, S., Fressengeas, C., 2015. A numerical spectral approach to solve the dislocation density transport equation. *Modelling Simul. Mater. Sci. Eng.* 23.
- Djaka, K.S., Villani, A., Taupin, V., Capolungo, L., Berbenni, S., 2017. Field dislocation mechanics for heterogeneous elastic materials: a numerical spectral approach. *Comput. Methods Appl. Mech. Engrg.* 315, 921–942.
- Espinosa, H., Panico, M., Berbenni, S., Schwarz, K., 2006. Discrete dislocation dynamics simulations to interpret plasticity size and surface effects in freestanding fcc thin films. *Int. J. Plast.* 22.
- Forest, S., Guéninchault, N., 2013. Inspection of free energy functions in gradient crystal plasticity. *Acta Mech. Sin.* 29.
- Frank, F., 1950. A Symposium on the Plastic Deformation of Crystalline Solids: Mellon Institute, vol. 834, US Government Printing Office, Pittsburgh.
- Fressengeas, C., Taupin, V., Capolungo, L., 2011. An elasto-plastic theory of dislocation and disclination fields. *Int. J. Solids Struct.* 48 (25–26), 3499–3509.
- Fressengeas, C., Taupin, V., Capolungo, L., 2014. Continuous modeling of the structure of symmetric tilt boundaries. *Int. J. Solids Struct.* 51.
- Grimmer, H., 1974. A reciprocity relation between the coincidence site lattice and the DSC lattice. *Scr. Metall.* 8.
- Guénol, J., Nöhring, W.G., Vaid, A., Houllé, F., Xie, Z., Prakash, A., Bitzek, E., 2020. Assessment and optimization of the fast inertial relaxation engine (fire) for energy minimization in atomistic simulations and its implementation in lammmps. *Comput. Mater. Sci.* 175, 109584.
- Guénol, J., Taupin, V., Vallet, M., Yu, W., Guitton, A., 2022. Features of a nano-twist phase in the nanolayered Ti_3AlC_2 MAX phase. *Scr. Mater.* 210.
- Hartley, C., Mishin, Y., 2005. Characterization and visualization of the lattice misfit associated with dislocation cores. *Acta Mater.* 53 (5), 1313–1321.
- Heinonen, V., Achim, C., Elder, K., Buyukdagli, S., Ala-Nissila, T., 2014. Phase-field-crystal models and mechanical equilibrium. *Phys. Rev. E* 89.
- Hirel, P., 2015. Atomsk: A tool for manipulating and converting atomic data files. *Comput. Phys. Comm.* 197.
- Jafari, M., Jamshidian, M., Ziaei-Rad, S., Raabe, D., Roters, F., 2017. Constitutive modeling of strain induced grain boundary migration via coupling crystal plasticity and phase-field methods. *Int. J. Plast.* 99.
- Jebahi, M., Cai, L., Abed-Meraim, F., 2020. Strain gradient crystal plasticity model based on generalized non-quadratic defect energy and uncoupled dissipation. *Int. J. Plast.* 126.
- Kresse, G., Hafner, J., 1993. Ab initio molecular dynamics for liquid metals. *Phys. Rev. B* 47.
- Kröner, E., 1980. Continuum model of defects. In: Balian, R., et al. (Eds.), *Physics of Defects*, Physics of Defects. 218.
- Lu, S., Zhao, J., Huang, M., Li, Z., Kang, G., Zhang, X., 2022. Multiscale discrete dislocation dynamics study of gradient nano-grained materials. *Int. J. Plast.* 156.
- Miehe, C., Aldakheel, F., Raina, A., 2016. Phase field modeling of ductile fracture at finite strains: A variational gradient-extended plasticity-damage theory. *Int. J. Plast.* 84.
- Mishin, Y., Mehl, M., Papaconstantopoulos, D., Voter, A., Kress, J., 2001. Structural stability and lattice defects in copper: Ab initio, tight-binding, and embedded-atom calculations. *Phys. Rev. B* 63 (22), 224106.
- Mura, T., 1963. Continuous distribution of moving dislocations. *Phil. Mag.* 8.
- Nye, J.F., 1953. Some geometrical relations in dislocated crystals. *Acta Metall.* 1.
- Priester, L., 2012. Grain Boundaries: From Theory to Engineering, vol. 172, Springer Science & Business Media.
- Read, W.T., Shockley, W., 1950. Dislocation models of crystal grain boundaries. *Phys. Rev.* 78, 275.
- Seif, D., Po, G., Mrovec, M., Lazar, M., Elsässer, C., Gumbsch, P., 2015. Atomistically enabled nonsingular anisotropic elastic representation of near-core dislocation stress fields in α -iron. *Phys. Rev. B* (18), 184102.
- Stukowski, A., 2009. Visualization and analysis of atomistic simulation data with OVITO—the Open Visualization Tool. *Modelling Simul. Mater. Sci. Eng.* 18.
- Taupin, V., Capolungo, L., Fressengeas, C., 2014. Disclination mediated plasticity in shear-coupled boundary migration. *Int. J. Plast.* 53, 179–192.
- Taupin, V., Capolungo, L., Fressengeas, C., Das, A., Upadhyay, M., 2013. Grain boundary modeling using an elasto-plastic theory of dislocation and disclination fields. *J. Mech. Phys. Solids* 61.
- Thompson, A.P., Aktulga, H.M., Berger, R., Bolintineanu, D.S., Brown, W.M., Crozier, P.S., in't Veld, P.J., Kohlmeyer, A., Moore, S.G., Nguyen, T.D., et al., 2022. LAMMPS—a flexible simulation tool for particle-based materials modeling at the atomic, meso, and continuum scales. *Comput. Phys. Comm.* 271.
- Trautt, Z., Adland, A., Karma, A., Mishin, Y., 2012. Coupled motion of asymmetrical tilt grain boundaries: Molecular dynamics and phase field crystal simulations. *Acta Mater.* 60.
- Tschopp, M.A., Coleman, S.P., McDowell, D.L., 2015. Symmetric and asymmetric tilt grain boundary structure and energy in cu and al (and transferability to other fcc metals). *Integr. Mater. Manuf. Innov.* 4, 176–189.
- Van Beers, P., Kouznetsova, V., Geers, M., Tschopp, M., McDowell, D., 2015. A multiscale model of grain boundary structure and energy: From atomistics to a continuum description. *Acta Mater.* 82.
- Weinberger, C.R., Tucker, G.J., 2016. Multiscale materials modeling for nanomechanics.
- Winter, I.S., Opperstrup, T., Frolov, T., Rudd, R., 2022. Characterization and visualization of grain boundary disconnections. *Acta Mater.* 237.
- Xu, C., Tian, X., Jiang, W., Wang, Q., Fan, H., 2022. Atomistic migration mechanisms of $[12\bar{1}0]$ symmetric tilt grain boundaries in magnesium. *Int. J. Plast.* 156, 103362.
- Zhang, X., Acharya, A., Walkington, N.J., Bielak, J., 2015. A single theory for some quasi-static, supersonic, atomic, and tectonic scale applications of dislocations. *J. Mech. Phys. Solids* 84.